SIMULATION OF PHYSICAL PROCESSES

Original article
DOI: https://doi.org/10.18721/JPM.18402

DEVELOPMENT OF AN ELASTIC MODEL FOR THE EPITAXIAL THIN FILM OF LEAD ZIRCONATE CONSIDERING INTERFACIAL MICRO-TWISTS

I. V. Khlyupin✉, *V. R. Meshkov*, *D. A. Sokolova*, *R. G. Burkovsky*

Peter the Great St. Petersburg Polytechnic University, St. Petersburg, Russia

✉ hlyupin.iv@yandex.ru

Abstract. The aim of this work was to develop a model to describe some microscopic phenomena in the epitaxial thin films based on lead zirconate $PbZrO_3$. The model takes into account the epitaxial contact of the film with the substrate and conditions for mechanical compatibility of the domains. It includes contributions from pseudopolarization, elastic and domain-domain interactions as well as a contribution analogous to electrostriction in ferroelectric materials. The parameter optimization has been performed through free energy minimization with varying the magnitudes of elastic displacements and the pseudopolarization vectors. The results obtained qualitatively reproduced a part of the experimental observations on the domain matching in the thin films, to be exact, the change in microscopic twisting in the domain wall regions when removing the epitaxial structure away from the substrate.

Keywords: antiferroelectrics, epitaxial thin films, pseudopolarization, free energy, gradient descent method

Funding: The reported study was funded by Russian Science Foundation (Project No. 20-72-10126).

Citation: Khlyupin I. V., Meshkov V. R., Sokolova D. A., Burkovsky R. G., Development of an elastic model for the epitaxial thin film of lead zirconate considering interfacial micro-twists, St. Petersburg State Polytechnical University Journal. Physics and Mathematics. 18 (4) (2025) 21–33. DOI: https://doi.org/10.18721/JPM.18402

This is an open access article under the CC BY-NC 4.0 license (https://creativecommons.org/licenses/by-nc/4.0/)

Научная статья
УДК 538.913
DOI: https://doi.org/10.18721/JPM.18402

РАЗРАБОТКА УПРУГОЙ МОДЕЛИ ЭПИТАКСИАЛЬНОЙ ТОНКОЙ ПЛЕНКИ ЦИРКОНАТА СВИНЦА С УЧЕТОМ ПРИИНТЕРФЕЙСНЫХ МИКРОСКРУЧИВАНИЙ

И. В. Хлюпин✉, *В. Р. Мешков*, *Д. А. Соколова*, *Р. Г. Бурковский*

Санкт-Петербургский политехнический университет Петра Великого, Санкт-Петербург, Россия

✉ hlyupin.iv@yandex.ru

Аннотация. Цель работы – построение модели для описания микроскопических скручиваний в эпитаксиальных тонких пленках на основе цирконата свинца $PbZrO_3$. Модель описывает эпитаксиальный контакт пленки с подложкой и условия механической совместимости доменов, вклады от псевдополяризации, упругих и

© Khlyupin I. V., Meshkov V. R., Sokolova D. A., Burkovsky R. G., 2025. Published by Peter the Great St. Petersburg Polytechnic University.

домен-доменных взаимодействий, а также вклад от аналога электрострикции в сегнетоэлектрических материалах. Оптимизация значений параметров осуществлялась через минимизацию свободной энергии при варьировании величины упругих смещений и векторов псевдополяризации. Полученные результаты качественно воспроизвели часть экспериментальных наблюдений по стыковке доменов в изучаемых пленках, а именно – изменение микроскопических скручиваний в области доменных стенок при удалении эпитаксиальной структуры от ее подложки.

Ключевые слова: антисегнетоэлектрик, эпитаксиальная тонкая пленка, псевдополяризация, свободная энергия, метод градиентного спуска

Финансирование: Работа выполнена при поддержке Российского научного фонда (проект № 20-72- 10126).

Ссылка для цитирования: Хлюпин И. В., Мешков В. Р., Соколова Д. А., Бурковский Р. Г. Разработка упругой модели эпитаксиальной тонкой пленки цирконата свинца с учетом приинтерфейсных микроскручиваний // Научно-технические ведомости СПбГПУ. Физико-математические науки. 2025. Т. 18. № 4. С. 21–33. DOI: https://doi.org/10.18721/JPM.18402

Статья открытого доступа, распространяемая по лицензии CC BY-NC 4.0 (https://creativecommons.org/licenses/by-nc/4.0/)

Introduction

Antiferroelectrics are crystalline compounds where antiparallel orientation of electric dipole moments of neighboring ions is observed within a certain temperature range. Ferroelectrics are crystalline compounds where spontaneous polarization is observed even in the absence of an external electric field. These two types of materials are closely related in many ways, but the former are studied in less detail. However, antiferroelectrics have already found practical applications, for example, as dielectrics in manufacturing of capacitors. Antiferroelectrics are approaching practical application in other areas: with active research focused on using these materials in data storage and energy storage [1–4].

The special properties of these two types of materials are due to their domain structure. In the case of ferroelectrics, a domain is defined as a region with uniform ordering of the dipole moments of unit cells. The presence of an uncompensated electric dipole moment in the unit cell results in macroscopic polarization. In contrast, for antiferroelectrics, the domains cannot be characterized only in terms of polarization: an additional characteristic, antipolarization, has to be introduced [5]. The latter implies an oppositely directed polarization in neighboring unit cells, leading to zero macroscopic polarization.

Numerous models were constructed to describe the properties of monocrystalline ferroelectric and antiferroelectric materials [5–10]. Most of them are based on Landau's phenomenological theory. Polarization and antipolarization, as well as deformation of the crystal lattice, are used as order parameters to describe the free energy of antiferroelectrics [5].

However, there are currently no models consistent with experimental observations of domain interactions in thin antiferroelectric films. As advances are made in electronic technology, there is a rising need to explore epitaxial thin-film structures for predicting the properties of nanostructures and minimizing costly experiments. Such models can help interpret complex phenomena characteristic of thin epitaxial structures in antiferroelectrics [6, 11–13]. Consequently, developing these models is a critical objective.

A recent study of the epitaxial $PbZrO_3$ thin film [12] experimentally observed the broadening of superstructural reflections. This effect was observed for the first time; the authors attributed it to the constraint imposed by the substrate, which prevents the domains in the film from achieving full mechanical compatibility, resulting in the formation of micro-twists near the interface.

This experimental study of epitaxial thin films of lead zirconate served as the starting point for our paper.

© Хлюпин И. В., Мешков В. Р., Соколова Д. А., Бурковский Р. Г., 2025. Издатель: Санкт-Петербургский политехнический университет Петра Великого.

The goals of this study were to construct a model of microstructural phenomena in epitaxial thin films of lead zirconate to analyze the effect of the substrate on the coexistence of domains, and to evaluate the applicability of the proposed model by reproducing the experimental observations.

The model is based on Landau's phenomenological theory of phase transitions. We considered the $PbZrO_3$ crystal in the context of ferroelastic distortions occurring in its structure; the model introduces pseudopolarization as an auxiliary order parameter. This parameter is used instead of the previous antipolarization parameter to simplify the model: it corresponds to higher-level domain structures. If a certain antipolarization direction corresponds to the directions of ion shifts in $PbZrO_3$ domains, then a certain pseudopolarization direction corresponds to clusters of domains with nearly identical spontaneous strain tensors. This approach is more convenient if only elastic effects are considered.

The optimal parameters of the model were determined by minimizing the free energy so that numerically calculated lattice constant ratios would reproduce the experimentally found values.

Free energy model

The basis for our model is the Landau phenomenological theory with a single order parameter, as applied to $BaTiO_3$ in [10]. The pattern of antiferroelectric domains in $PbZrO_3$ crystals is very complex, while ferroelastic distortions are far simpler to describe. Pseudopolarization was chosen in our model as the order parameter to account for ferroelastic distortions.

This order parameter is distinct from polarization in that it does not generate depolarizing fields. This is an abstract order parameter, which we believe occurs in a lead zirconate crystal during the phase transition from a paraelectric phase to an antiferroelectric one.

The occurrence of spontaneous pseudopolarization leads to a lowering of the crystal symmetry from cubic to tetragonal. This symmetry is higher than the real one in $PbZrO_3$ (which is orthorhombic), but it corresponds to the real spontaneous strain tensor of the orthorhombic phase with acceptable accuracy.

The unit cell of orthorhombic symmetry should be regarded as pseudotetragonal, with crystal lattice constants

$$a_{pt} = a_0/\sqrt{2} \approx b_0/2\sqrt{2},\ c_{pt} = c_0/\sqrt{2},$$

where a_0, b_0, c_0 are the constants of the orthorhombic lattice; a_{pt}, c_{pt} are the constants of the pseudotetragonal lattice [12].

Thus, our description is similar to the model in [10] for ferroelectric materials, except that the proposed description lacks the term responsible for depolarizing fields.

The direction of pseudopolarization is set to be coaxial with c_{pt} in the pseudotetragonal approximation of the crystal lattice. The lattice constant ratio along the **a** and **b** axes is 1:2, while the lattice constant in the direction of the ***c*** axis is 1% smaller than in the direction of the **a** axis. For this reason, the mechanical compatibility of antiferroelectric domains appears significantly compromised only if the domains have oppositely oriented **c** axes.

Let us consider the possible antiferroelectric domain configurations in more detail to clarify the nature of domains characterized by pseudopolarization. The antiferroelectric domain structures in lead zirconate are hierarchical and highly complex. Six orientation states are possible in the orthorhombic phase with four translational states possible for each. As a result, there are 24 possible domain states. Structures consisting of domains that differ only in translation are the simplest. For example, following along the **b** axis, we observe lead ion shifts in an up-up-down-down pattern. When this pattern is locally disrupted by a change in the phase of the modulation wave, for instance, due to an extra 'down' shift, an antiphase domain wall forms, located perpendicular to the **b** axis. These walls are separated by domains with the same orientation and different translational states (simplistically called antiphase domains). Such domains are identical in terms of spontaneous strains. More complex domain structures are at the boundaries between regions filled with antiphase domain structures. The simplest case are 90-degree domain boundaries, when the **b** axes on different sides of the domain wall are oriented at a right angle. Formally, the domains on different sides of such a wall differ by spontaneous strains. However, in practice, this difference turns out to be small, since the **b**-axis lattice parameter equals twice the **a**-axis lattice parameter with sufficiently high accuracy (see above). Clusters of such 90-degree domains are characterized by a single direction of the **c** axis. Spontaneous strains become significant at the

boundaries between clusters of 90-degree domains with different directions of the **c** axis, since the lattice parameter of this axis differs substantially (by 1%) from $a/\sqrt{2}$ and $b/2\sqrt{2}$.

This clarification leads to the following statement: within the ferroelastic description, a domain is a cluster of 90-degree antiferroelectric domains with a common **c** axis along which the pseudopolarization vector is directed.

The formula for the total energy taking into account phenomena of different nature is as follows:

$$F = \int \left[f_L^{(e)}(P_i) + f_C(e_{ij}) + f_q(P_i, e_{ij}) + f_G(P_{i,j}) \right] dV, \quad (1)$$

where f_L, f_C, f_G are the contributions from pseudopolarization, from purely elastic interactions, from domain–domain interactions, respectively; f_q is the contribution similar to that from electrostriction in ferroelectric materials; P_i is the component of the pseudopolarization field vector; $P_{i,j}$ is the derivative of the pseudopolarization vector components along different directions; e_{ij} is the elastic stress field.

The energy f_G is equal to zero for regions with homogeneous pseudopolarization and strain (monodomains), since it depends only on the gradients of these fields. Values other than zero appear at domain boundaries (domain walls), and therefore it is appropriate to refer to this energy component as the energy of the domain–domain interaction. It can be seen from the formula that the energy is determined by the pseudopolarization field, its gradient, and the elastic stress field. The field e_{ij} depends on the elastic displacement field u_i by the following formula:

$$e_{i,j} = (u_{i,j} + u_{j,i})/2,$$

where i, j are the indices for the directions of the 3D space corresponding to the directions of the coordinates x, y, z; $i, j = \{1, 2, 3\}$.

The total energy of the crystal is given as the integral of the sum of the contributions over the entire crystal. The presented model is a continuum model based on a grid with a 1 nm spacing. In the absence of distortions, this grid corresponds to the cubic phase. The grid is distorted with a change in symmetry so that the aspect ratios reflect the ratios of the new lattice constants.

According to [14], the formula for calculating the contribution F_L from one order parameter for a certain region of the crystal has the following form:

$$\begin{aligned} f_L^{(e)}(P_i) = {} & a_1(P_1^2 + P_2^2 + P_3^2) + \\ & + a_{11}(P_1^4 + P_2^4 + P_3^4) + \\ & + a_{12}(P_1^2 P_2^2 + P_1^2 P_3^2 + P_2^2 P_3^2) + \\ & + a_{111}(P_1^6 + P_2^6 + P_3^6) + \\ & + a_{112}\left[P_1^4(P_2^2 + P_3^2) + P_2^4(P_1^2 + P_3^2) + P_3^4(P_1^2 + P_2^2) \right] + \\ & + a_{123} P_1^2 P_2^2 P_3^2, \end{aligned}$$

where α_i, α_{ij}, α_{ijk} are the coefficients of the Landau–Devonshire potential for pseudopolarization.

The following formula was used to calculate the contribution from elastic energy in a certain region of the crystal [10]:

$$\begin{aligned} f_C(e_{ij}) = {} & \frac{1}{2} C_{11}({e_{11}}^2 + {e_{22}}^2 + {e_{33}}^2) + \\ & + C_{12}(e_{22}e_{33} + e_{11}e_{33} + e_{11}e_{22}) + \\ & + 2C_{44}({e_{23}}^2 + {e_{13}}^2 + {e_{12}}^2), \end{aligned}$$

where C is the stiffness tensor (its components C_{11}, C_{12}, C_{44}, given in Voigt notation, were selected in accordance with the data in [15] based on the cubic symmetry of the initial crystal).

The contribution from elastic-pseudopolarization coupling was calculated by the formula [10]:

$$f_q(P_i, e_{ij}) = -q_{11}\left(e_{11}P_1^2 + e_{22}P_2^{\,2} + e_{33}P_3^{\,2}\right) -$$
$$-q_{12}\left[e_{11}\left(P_2^{\,2} + P_3^{\,2}\right) + e_{22}\left(P_1^2 + P_3^{\,2}\right) + e_{33}\left(P_1^2 + P_2^{\,2}\right)\right] -$$
$$-2q_{44}\left(e_{12}P_1P_2 + e_{13}P_1P_3 + e_{23}P_2P_3\right)$$

For ferroelectric crystals, the term f_q takes into account the influence of the electrostrictive coupling tensor q determining the magnitude and direction of elastic strain of the crystal lattice. Within our proposed model, the term f_q determines a similar effect in an antiferroelectric crystal due to pseudopolarization.

The ratio from [10] was used to determine the energy of the domain walls in the crystal:

$$f_G\left(P_{i,j}\right) = \frac{1}{2}G_{11}\left(P_{1,1}^2 + P_{2,2}^2 + P_{3,3}^2\right) +$$
$$+G_{14}\left(P_{1,1}P_{2,2} + P_{2,2}P_{3,3} + P_{1,1}P_{3,3}\right) +$$
$$+\frac{1}{2}G_{44}\left(P_{1,2}^2 + P_{2,1}^2 + P_{2,3}^2 + P_{3,2}^2 + P_{3,1}^2 + P_{1,3}^2\right).$$

Therefore, in addition to the pseudopolarization parameter P, four groups of parameters can be distinguished in our proposed model:

parameters C_{11}, C_{12} and C_{44}, describing the elastic interactions of neighboring atoms;

parameters α_1, α_{11}, α_{12}, α_{111}, α_{112} and α_{123}, determining the magnitude and direction of the pseudopolarization vector **P**;

parameters q_{11}, q_{12} and q_{44}, governing the coupling between elastic displacements u and pseudopolarization P;

parameters G_{11}, G_{14} and G_{44}, determining the interaction of neighboring atoms occurring with a spatial gradient of the pseudopolarization vector **P**.

Software implementation of the proposed model

Optimization of the energy function was carried out using the gradient descent method. In our case, optimization means minimizing the free energy function by varying the magnitude of elastic displacements u and pseudopolarization P with other parameters fixed. To simulate the constraints imposed by the substrate, we introduced boundary conditions at the lower interface of the crystal corresponding to compressive or tensile epitaxial strain from the substrate. Next, to fix the epitaxial layer in the initial position, we assumed the elastic displacement gradient at the lower interface to equal zero throughout the entire optimization procedure.

The gradient descent step size was adjusted automatically from the initial guess based on the maximum gradient value, increased or decreased until the energy assumed a constant value along the optimization path.

The gradient could be calculated by a simpler approach introducing cyclic boundary conditions in the x and y directions. However, this is impossible in this case due to the condition for epitaxial strain, inducing a mismatch between the atomic positions at the layer boundaries. Due to this obstacle, we had to increase the number of atoms included in the simulation, analytically calculating the spatial gradient of the energy function to accelerate the optimization procedure.

Simulation results

One of the goals of our study was to assess whether the proposed model was applicable to describing the coexistence of domains in antiferroelectric thin films based on $PbZrO_3$. The films were oriented with the [0 0 1] direction normal to the surface and grown on a strontium titanate ($SrTiO_3$) substrate. The samples were chosen because their domain structure was known, since we analyzed these heterostructures earlier (see [11, 12]) via single-crystal XRD. In our mathematical representation, the system is modeled as a grid whose bottom layer describes the substrate. The substrate is clamped, while the rest of the grid representing the film is arranged in accordance with

the model. In our computational approach, the grid was not explicitly bound to the atomic sites of the substrate or film lattice. Instead, the system was represented by a cubic region of the crystal with a side length of 1 nm. In this case, the displacements and pseudopolarization at a given point are treated as the averages for the atoms within this region, allowing for small fluctuations.

The initial parameter values were taken for the $BaTiO_3$ ferroelectric from [10]. We believe that this approach is acceptable because the parameter values for antiferroelectrics should be close to those for ferroelectrics, due to the related nature of the materials. Indeed, antiferroelectric and ferroelectric crystals exhibit nearly identical properties under certain conditions, for example, in highly symmetric phases (apparently, the values of the parameters for describing them should be close as well). On the other hand, the proposed model considers ferroelastic crystal distortions instead of the antiferroelectric domain pattern; therefore, the characteristics of perovskite ferroelectric materials can also be used.

The initial pseudopolarization value was also assumed to be zero, which is equivalent to the case of a lead zirconate crystal in cubic phase with a lattice constant a = 4.15 Å [16]. The parameter values were optimized in several stages, with the optimal values of one or more groups of model parameters determined at each stage. In our case, it is impossible to fully verify the obtained parameter values, since no experiments were conducted to obtain these parameters specifically for $PbZrO_3$ films. Thus, the criteria for achieving optimal parameter values were based on the similarity of the parameters of the modeled structure with the experimental data.

At the *first stage*, we tested the feasibility of using the initial values for the components of the stiffness tensor C (C_{11}, C_{12} and C_{44}), taken from the model for the $BaTiO_3$ ferroelectric in [10]). The criterion for using these values was the relaxation of the film lattice constant. Specifically, we verified that the lattice parameter tended toward the value characteristic for a bulk single crystal with increasing distance from the substrate. Consequently, the following numerical values were obtained for the components of the stiffness tensor C:

Parameter	Value, nJ·m^{-3}
C_{11}	2.750
C_{12}	1.790
C_{44}	0.543

Fig. 1 shows the variation in the parameter ρ (average distance between adjacent layers) depending on the distance from the substrate. The parameter ρ follows a normalized expression of the form

$$\rho = (L_{i+1} - L_i)/a,$$

where L_i, L_{i+1} are the average atomic coordinates of the ith and $(i+1)$th layers in the z direction, respectively, with increasing distance from the substrate, a is the lattice constant.

It can be seen from this formula and from Fig. 1 that the relaxation condition is expressed by the equation ρ = 1. The parameter ρ increases uniformly with increasing distance from the substrate: the ρ value near the substrate–film interface is less than unity due to lattice constant mismatch between the film and the substrate. However, the parameter ρ becomes equal to unity after the 13th atomic layer, i.e., the distance between the layers returns to the case of an undeformed single crystal. Notably, the numerical values taken by the components of the stiffness tensor C, selected by minimization and presented above, coincide with the numerical values obtained from the model for the $BaTiO_3$ ferroelectric (see [10]). Thus, it is proved that the values of the stiffness tensor components are applicable to the case of antiferroelectric $PbZrO_3$ films.

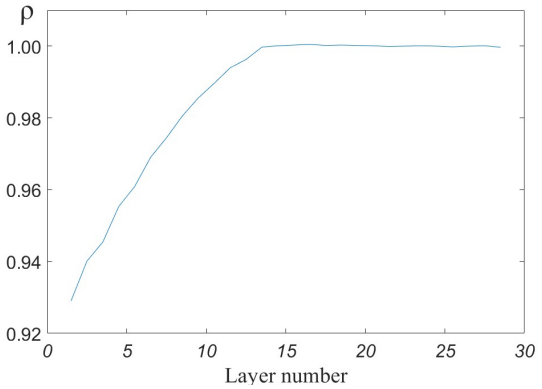

Fig. 1. Calculated dependence of averaged interlayer spacing in antiferroelectric $PbZrO_3$ films on the distance from $SrTiO_3$ substrate

At the *second stage* of the simulation, we determined the optimal values for the components of the domain interaction tensor (α) and the elastic-pseudopolarization coupling tensor (*q*) using the components of the stiffness tensor *C* obtained at the first stage of the simulation. The parameters α_i, α_{ij}, α_{ijk}, *q* and *P* are responsible for the difference between the cubic and antiferroelectric orthorhombic phases of $PbZrO_3$; the unit cell of the second phase can be regarded as pseudotetragonal [17]. The lowering of the symmetry in the lead zirconate structure is caused by the displacement of several groups of atoms from their positions in the cubic phase and the emergence of accompanying internal stresses. As for the behavior of the coordinate grid nodes, the transition to the antiferroelectric phase results in a 1% compression of the unit cell (relative to the cubic phase) along the pseudopolarization vector. Consequently, new parameters of the $PbZrO_3$ cell in the pseudotetragonal representation should take the values $a \approx b \approx 4.16$ Å, $c \approx 4.11$ Å. It was observed in [12] for $PbZrO_3$ thin films with the normal oriented along the [0 0 1] direction that the shorter axis of the pseudotetragonal unit cell can only lie in the film plane. Therefore, we selected such values for the components of the parameter α at which the pseudopolarization vector would be oriented along the [1 0 0] direction. The values of the *q* tensor components were chosen so as to reproduce the 1% compressive strain of the film lattice. Thus, at the second stage of simulation, we obtained the optimal values of the parameters α_i, α_{ij}, α_{ijk} and *q* at which the film's unit cell was compressed by 1% along the direction of the pseudopolarization vector. The obtained numerical values of the parameters α_i, α_{ij}, α_{ijk} и *q* are given in Table.

At the *third stage* of the simulation, we determined the optimal values of the parameters G_{11}, G_{14} and G_{44}. For this purpose, we introduced the domain wall, considering its motion under epitaxial strain induced by the substrate. We adopted the simplest configuration with two domains initially separated by a domain wall located at a 45° angle to the pseudopolarization vector. Such an orientation of the domain wall was chosen because this specific configuration is mechanically compatible in the free-standing film (i.e., not in contact with the substrate). In other words, the domains can be connected in this crystal configuration without inducing strain [12]. Notably, the size of the domains was not taken into account at the third stage of the simulation. Strictly speaking, it is not entirely correct to use a two-domain configuration, since there are typically more than two domains and their sizes can vary significantly [18]. However, more complex domain configurations remained beyond the scope of this study as they are technically challenging to implement in the current model.

Table

Optimization of key system parameters

Parameter	Value	Unit
α_1	–3.98	10^7 J·m·C^{-2}
α_{11}	6.723	10^8 J·m^5·C^{-4}
α_{12}	5.32	10^8 J·m^5·C^{-4}
α_{111}	1.15	10^9 J·m^{-9}·C^{-6}
α_{112}	–2.46	10^9 J·m^{-9}·C^{-6}
α_{123}	–2.28	10^9 J·m^{-9}·C^{-6}
q_{11}	–5.61	10^9 J·m·C^{-2}
q_{12}	–3.7	10^9 J·m·C^{-2}
q_{44}	1.41	10^9 J·m·C^{-2}

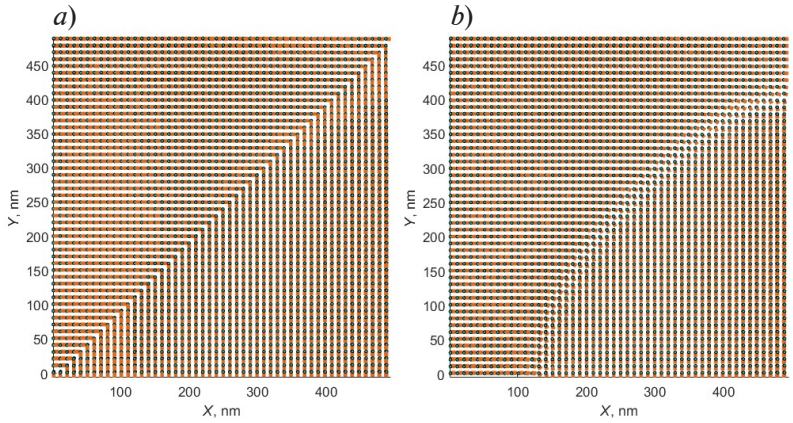

Fig. 2. 2D patterns of pseudopolarization vector orientation in the crystal (top views): initial conditions (*a*), after optimization by the model adopted (*b*)

The criterion for optimizing the parameter at this stage was to preserve the two-domain configuration with the width of the domain wall not exceeding several lattice spacings. Fig. 2 shows 2D patterns for the initial orientations of the pseudopolarization vectors **P** (before free energy optimization in accordance with the model (Fig. 2,*a*)) and the corresponding orientations of the pseudopolarization vectors after free energy optimization in accordance with the model (Fig. 2,*b*). Evidently, optimization of the parameters leads to curvature of the domain wall. We understand the curvature of the domain wall as nothing more than an optimization artifact occurring due to relatively small grid sizes.

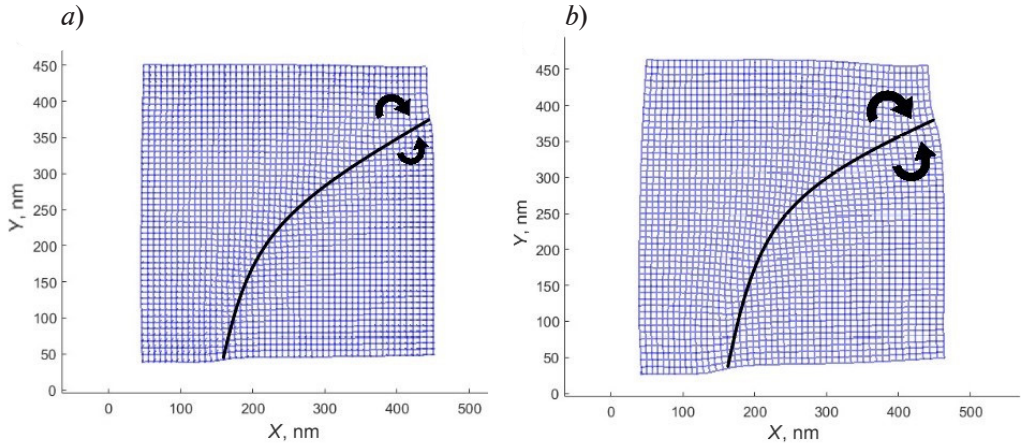

Fig. 3. 2D strain maps for film layers located three (*a*) and ten (*b*) atomic spacings away from the substrate. For clarity, the deformation in the layers is magnified by 20 times. The arrows show the directions of rotation of the domains near the domain wall

Fig. 3 illustrates two cases of deformation in different film layers, taking into account all contributions to the free energy of the system. The shifts in the atomic positions are magnified, making it possible to clearly visualize the deformation of the crystal, even though the actual strain magnitude changes by less than 1%. The patterns reveal deformation in the shape of the crystal arising from the mismatch between the shapes of the domains with different orientation of the polarization vector. The difference in the shapes produces strains near the domain wall. The strain amplitudes are not the same for different layers of the crystal: strains with smaller amplitude are observed closer to the substrate. As seen from the deformation pattern, the domains rotate in opposite directions relative to the domain wall, and their rotation clearly reproduces the experimentally observed ‘clapping’ of the domains, described in [12]. For comparison with the experimental data from [12], we calculated the clapping angles for different layers of the film.

The clapping angle 2φ was calculated by the formula

$$2\varphi = |\Delta c - \Delta a|/a_c,$$

where $\Delta c = c_{pt} - a_c$, $\Delta a = a_{pt} - a_c$; the product a_c is defined as $(a_{pt} + c_{pt})/2$. The subscript *pt* corresponds to the parameters of the pseudotetragonal lattice, and the subscript *c* to the parameters of the cubic lattice.

The clapping angles obtained from the model data vary, depending on the specific layer: the angle is $2\varphi = 0.0021$ near the interface between the substrate and the film, $2\varphi = 0.0057$ in the third layer, $2\varphi = 0.0095$ in the tenth layer. The clapping angle virtually does not change with subsequent distance from the substrate. The angle 2φ for the relaxed film (thirteenth layer and beyond) turned out to be quite close to the experimental observations [12], according to which $2\varphi = 0.0097°$.

Thus, the clapping angle is different for layers close to the substrate and tends to the theoretical value in a single crystal. The numerical values of the components of the domain-domain interaction tensor *G*, found at the third stage, are given below.

Parameter	Value, $pJ \cdot m^3 \cdot C^{-2}$
G_{11}	320
G_{14}	0
G_{44}	100

Conclusion

We describe the domain interactions in antiferroelectric epitaxial structures by decomposing the free energy into several contributions. These include contributions from pseudopolarization, purely elastic interactions, interactions between domains with different pseudopolarization vectors, interactions of elastic displacements, and a contribution similar to that from electrostriction in ferroelectric materials. The coefficients for various contributions to the total energy were selected so that the calculated results were at least qualitatively consistent with the experimental observations.

Ultimately, our results qualitatively reproduce some of the experimental observations on domain matching in $PbZrO_3$ thin films: the mechanical compatibility of the domains is compromised by the substrate, which is expressed in the variation in the clapping angle with distance from the substrate interface.

The obtained simulation results are in good agreement with experimental data, indicating that the model is effective for describing such effects.

The proposed model is preliminary and, in our opinion, requires further refinement. Simulation can be improved by refining the boundary conditions that account for the interactions of the film with the substrate and the ambient environment. In addition, the model parameters should be adjusted experimentally, making it possible to reproduce multidomain cases and their structures in crystalline compounds with greater accuracy. To model these systems, particularly larger-scale features like stripe domain series in epitaxial heterostructures, the simulation results must be validated and the optimization approach further developed.

REFERENCES

1. **Morris D. H., Avci U. E., Young I. A.,** Anti-ferroelectric capacitor memory cell: US Patent No. 11,355,504 B2, filed May 31, 2018, published Jun. 7, 2022. Assignee: Intel Corporation, USA.

2. **Pesic M., Knebel S., Hoffmann M., et al.,** How to make DRAM non-volatile? Anti-ferroelectrics: A new paradigm for universal memories, Proc. 2016 IEEE Int. Electron Devices Meeting (IEDM), Dec. 3–7, 2016. San Francisco, California, USA, IEEE (2016) 298–301.

3. **Zhang Y., Li X., Song J., et al.,** $AgNbO_3$ antiferroelectric film with high energy storage performance, J. Materiomics. 7 (6) (2021) 1294–1300.

4. **Huang X.-X., Zhang T.-F., Wang W., et al.,** Tailoring energy-storage performance in antiferroelectric $PbHfO_3$ thin films, Materials & Design. 204 (Jun) (2021) 109666.

5. **Haun M. J., Harvin T. J., Lanagan M. T., et al.,** Thermodynamic theory of $PbZrO_3$, J. Appl. Phys. 65 (8) (1989) 3173–3180.

6. **Chaudhuri A. R., Arredondo M., Нднnel A., et al.,** Epitaxial strain stabilization of a ferroelectric phase in $PbZrO_3$ thin films, Phys. Rev. B. 84 (5) (2011) 054112.

7. **Mtebwa M., Feigl L., Yudin P., et al.,** Room temperature concurrent formation of ultra-dense arrays of ferroelectric domain walls, Appl. Phys. Lett. 107 (14) (2015) 142903.

8. **Sawaguchi E.,** Ferroelectricity versus antiferroelectricity in the solid solutions of $PbZrO_3$ and $PbTiO_3$, J. Phys. Soc. Jpn. 8 (5) (1953) 615–629.

9. **Burkovsky R. G., Bronwald I., Andronikova D., et al.,** Triggered incommensurate transition in $PbHfO_3$, Phys. Rev. B. 100 (1) (2019) 014107.

10. **Marton P., Hlinka J.,** Simulation of domain patterns in $BaTiO_3$, Phase Transit. 79 (6–7) (2006) 467–483.

11. **Burkovsky R. G., Lityagin G. A., Ganzha A. E., et al.,** Field-induced heterophase state in $PbZrO_3$ thin films, Phys. Rev. B. 105 (12) (2022) 125409.

12. **Kniazeva M. A., Ganzha A. E., Gao R., et al.,** Highly mismatched antiferroelectric films: Transition order and mechanical state, Phys. Rev. B. 107 (18) (2023) 184113.

13. **Wei X.-K., Vaideeswaran K., Sandu C. S., et al.,** Preferential creation of polar translational boundaries by interface engineering in antiferroelectric $PbZrO_3$ thin films, Adv. Mater. Interf. 2 (18) (2015) 1500349.

14. **Pertsev N. A., Zembilgotov A. G., Tagantsev A. K.,** Effect of mechanical boundary conditions on phase diagrams of epitaxial ferroelectric thin films, Phys. Rev. Lett. 80 (9) (1998) 1988.

15. **Ostrosablin N. I.,** Symmetry classes of the anisotropy tensors of quasielastic materials and a generalized Kelvin approach, Appl. Mech. Tech. Phys. 58 (3) (2017) 469–488.

16. **Sawaguchi E., Shirane G., Takagi Y.,** Phase transition in lead zirconate, J. Phys. Soc. Jpn. 6 (5) (1951) 333–339.

17. **Corker D. L., Glazer A. M., Dec J., et al.,** A re-investigation of the crystal structure of the perovskite $PbZrO_3$ by X-ray and neutron diffraction, Acta Crystallogr. B. 53 (1) (1997) 135–143.

18. **Gonzales-Flores J. E., Ganzha A., Kniazeva M. A., et al.,** Thickness independence of antiferroelectric domain characteristic sizes in epitaxial $PbZrO_3/SrRuO_3/SrTiO_3$ films, J. Appl. Crystallogr. 56 (3) (2023) 697–706.

СПИСОК ЛИТЕРАТУРЫ

1. **Morris D. H., Avci U. E., Young I. A.** Anti-ferroelectric capacitor memory cell. Патент США № US 1135504 B2. Заявлен 31.05.2018; опубликован 07.06.2022; заявитель и патентообладатель – Intel Corporation, США. 25 с.

2. **Pesic M., Knebel S., Hoffmann M., Richter C., Mikolajick T., Shroeder V.** How to make DRAM non-volatile? Anti-ferroelectrics: A new paradigm for universal memories // Proceedings of the 2016 IEEE International Electron Devices Meeting (IEDM). December 3–7, 2016. San Francisco, California, USA. IEEE. 2016. Pp. 298–301.

3. **Zhang Y., Li X., Song J., Zhang S., Wang J., Dai X., Liu B., Dong G., Zhao L.** $AgNbO_3$ antiferroelectric film with high energy storage performance // Journal of Materiomics. 2021. Vol. 7. No. 6. Pp. 1294–1300.

4. **Huang X.-X., Zhang T.-F., Wang W., Ge P.-Z., Tang X.-G.** Tailoring energy-storage performance in antiferroelectric $PbHfO_3$ thin films // Materials & Design. 2021. Vol. 204. June. P. 109666.

5. **Haun M. J., Harvin T. J., Lanagan M. T., Zhuang Z. Q., Jang S. J., Cross L. E.** Thermodynamic theory of $PbZrO_3$ // Journal of Applied Physics. 1989. Vol. 65. No. 8. Pp. 3173–3180.

6. **Chaudhuri A. R., Arredondo M., Ндhnel A., Morelli A., Becker M., Alexe M., Vrejoiu I.** Epitaxial strain stabilization of a ferroelectric phase in $PbZrO_3$ thin films // Physical Review B. 2011. Vol. 84. No. 5. P. 054112.

7. **Mtebwa M., Feigl L., Yudin P., McJilly L. J., Shapovalov K., Tagantsev A. K., Setter N.** Room temperature concurrent formation of ultra-dense arrays of ferroelectric domain walls // Applied Physics Letters. 2015. Vol. 107. No. 14. P. 142903.

8. **Sawaguchi E.** Ferroelectricity versus antiferroelectricity in the solid solutions of $PbZrO_3$ and $PbTiO_3$ // Journal of the Physical Society of Japan. 1953. Vol. 8. No. 5. Pp. 615–629.

9. **Burkovsky R. G., Bronwald Iu., Andronikova D., et al.** Triggered incommensurate transition in $PbHfO_3$ // Physical Review B. 2019. Vol. 100. No. 1. P. 014107.

10. **Marton P., Hlinka J.** Simulation of domain patterns in $BaTiO_3$ // Phase Transitions. 2006. Vol. 79. No. 6–7. Pp. 467–483.

11. **Burkovsky R. G., Lityagin G. A., Ganzha A. E., Vakulenko A. F., Gao R., Dasgupta A., Xu B., Filimonov A. V., Martin L. W.** Field-induced heterophase state in $PbZrO_3$ thin films // Physical Review B. 2022. Vol. 105. No. 12. P. 125409.

12. **Kniazeva M. A., Ganzha A. E., Gao R., Dasgupta A., Filimonov A. V., Burkovsky R. G.** Highly mismatched antiferroelectric films: Transition order and mechanical state // Physical Review B. 2023. Vol. 107. No. 18. P. 184113.

13. **Wei X.-K., Vaideeswaran K., Sandu C. S., Jia Ch.-L., Setter N.** Preferential creation of polar translational boundaries by interface engineering in antiferroelectric $PbZrO_3$ thin films // Advanced Materials Interfaces. 2015. Vol. 2. No. 18. P. 1500349.

14. **Pertsev N. A., Zembilgotov A. G., Tagantsev A. K.** Effect of mechanical boundary conditions on phase diagrams of epitaxial ferroelectric thin films // Physical Review Letters. 1998. Vol. 80. No. 9. P. 1988.

15. **Остросаблин Н. И.** Классы симметрии тензоров анизотропии квазиупругих материалов и обобщение подхода Кельвина // Прикладная механика и техническая физика. 2017. Т. 58. № 3. С. 108–129.

16. **Sawaguchi E., Shirane G., Takagi Y.** Phase transition in lead zirconate // Journal of the Physical Society of Japan. 1951. Vol. 6. No. 5. Pp. 333–339.

17. **Corker D. L., Glazer A. M., Dec J., Roleder K., Whatmore R. W.** A re-investigation of the crystal structure of the perovskite $PbZrO_3$ by X-ray and neutron diffraction // Acta Crystallographica. Section B: Structural Science, Crystal Engineering and Materials. 1997. Vol. 53. No. 1. Pp. 135–143.

18. **Gonzales-Flores J. E., Ganzha A., Kniazeva M. A., et al.** Thickness independence of antiferroelectric domain characteristic sizes in epitaxial $PbZrO_3/SrRuO_3/SrTiO_3$ films // Journal of Applied Crystallography. 2023. Vol. 56. No. 3. Pp. 697–706.

THE AUTHORS

KHLYUPIN Ivan V.
Peter the Great St. Petersburg Polytechnic University 2
9 Politechnicheskaya St., St. Petersburg, 195251, Russia
hlyupin.iv@yandex.ru
ORCID: 0009-0000-7669-4705
MESHKOV Vadim R.
Peter the Great St. Petersburg Polytechnic University
29 Politechnicheskaya St., St. Petersburg, 195251, Russia
meshkovadim@yandex.ru ORCID: 0009-0009-2088-3932

SOKOLOVA Daria A.
Peter the Great St. Petersburg Polytechnic University
29 Politechnicheskaya St., St. Petersburg, 195251, Russia
kirpich_da@spbstu.ru
ORCID: 0009-0008-5965-3301

BURKOVSKY Roman G.
Peter the Great St. Petersburg Polytechnic University
29 Politechnicheskaya St., St. Petersburg, 195251, Russia
roman.burkovsky@gmail.com ORCID: 0000-0003-0474-3242

СВЕДЕНИЯ ОБ АВТОРАХ

ХЛЮПИН Иван Владимирович – *лаборант научно-образовательного центра «Физика нанокомпозитных материалов электронной техники» Института электроники и телекоммуникаций Санкт-Петербургского политехнического университета Петра Великого.*
195251, Россия, г. Санкт-Петербург, Политехническая ул., 29
hlyupin.iv@yandex.ru
ORCID: 0009-0000-7669-4705

МЕШКОВ Вадим Ростиславович – *кандидат технических наук, доцент Высшей школы теоретической механики и математической физики Физико-механического института Санкт-Петербургского политехнического университета Петра Великого.*
195251, Россия, г. Санкт-Петербург, Политехническая ул., 29
meshkovadim@yandex.ru
ORCID: 0009-0009-2088-3932

СОКОЛОВА Дарья Арнольдовна – *ассистент высшей инженерно-физической школы Института электроники и телекоммуникаций Санкт-Петербургского политехнического университета Петра Великого.*
195251, Россия, г. Санкт-Петербург, Политехническая ул., 29
kirpich_da@spbstu.ru
ORCID: 0009-0008-5965-3301

БУРКОВСКИЙ Роман Георгиевич – *кандидат физико-математических наук, доцент Высшей инженерно-физической школы Института электроники и телекоммуникаций Санкт-Петербургского политехнического университета Петра Великого.*
195251, Россия, г. Санкт-Петербург, Политехническая ул., 29
roman.burkovsky@gmail.com
ORCID: 0000-0003-0474-3242

Received 05.05.2025. Approved after reviewing 08.09.2025. Accepted 08.09.2025.
Статья поступила в редакцию 05.05.2025. Одобрена после рецензирования 08.09.2025. Принята 08.09.2025.

© Peter the Great St. Petersburg Polytechnic University, 2025